Optimized design and integration of energy storage in Solar-Assisted Ground-Source Heat Pump systems

Build Simul (2023) 16: 1933–1948
https://doi.org/10.1007/s12273-023-1030-4

Optimized design and integration of energy storage in Solar-Assisted Ground-Source Heat Pump systems

Maria Ferrara (✉), Enrico Fabrizio

Department of Energy, Politecnico di Torino, Turin, 10121, Italy

Research Article

Abstract

The integrated use of multiple renewable energy sources to increase the efficiency of heat pump systems, such as in Solar Assisted Geothermal Heat Pumps (SAGHP), may lead to significant benefits in terms of increased efficiency and overall system performance especially in extreme climate contexts, but requires careful integrated optimization of the different system components. In particular, thermal storages take a fundamental role in optimizing the integration of renewable energy sources and the system operation. This work investigates the potential design optimization of a SAGHP system in a mountain site by exploring many different alternatives to optimize the mutual relationship between the solar field, the geothermal field and the water thermal storages. This is done through an original simulation-based multi-objective optimization framework considering energy efficiency and economic feasibility, which allows appraising the impact of the different design alternatives on the overall system performance and on the dynamics of the different system components. Results identify a set of optimized system configurations that optimize the integrated exploitation of the different thermal sources showing a potential increase of the overall system performance leading to 34% lower global cost compared to the initial design. High robustness of the optimal design solutions is reported with respect to the current context of high economic uncertainty.

Keywords

thermal storage;
geothermal energy;
heat pumps;
building simulation;
artificial intelligence;
cost optimization;
energy flexibility

Article History

Received: 05 October 2022
Revised: 13 February 2023
Accepted: 10 April 2023

1 Introduction

According to latest IEA projections (International Energy Agency 2020), heat pump is a key clean energy technology that will drive decarbonization of the building sector in the next few years, especially relying on the integration of multiple renewable energy sources for increasing overall efficiency and applicability in different building typologies and boundary conditions (Alberti et al. 2018).

In general, it has been demonstrated that the combination of the solar and geothermal energy sources in Solar Assisted Ground-source Heat Pumps (SAGHP) (Ozgener and Hepbasli 2007) may potentially lead to multiple benefits in terms of increased global COP of the system (Wołoszyn and Gołaś 2017), and geothermal source regeneration for lower energy consumptions and higher renewable energy exploitation (Girard et al. 2015).

Thermal energy storages at both source and use sides is important for optimal integration of renewable energy sources considering their flexibility (Maturo et al. 2022), climate boundaries and economic feasibility (Osterman and Stritih 2021). In particular, economic feasibility is a key-point constituting a barrier for this technology for the large investment costs (Liu et al. 2021). Therefore, the optimization of the solar integration and of thermal storages is also crucial to reduce the size of the boreholes (Nouri et al. 2019), which are responsible for the higher costs related to this type of systems and may lead to high payback times unless tailored incentives and taxation policies are implemented (Rivoire et al. 2018).

Since the performance of such systems is complex and time variable in the long term (the thermal depletion of the ground can occur in a period of several years), it may not be sufficient to analyze short-term data available from monitoring but there is the need to use detailed transient simulation models for the design and optimization of the

E-mail: maria.ferrara@polito.it

Building Systems and Components

List of symbols

$C_{a,i}(j)$	annual cost for component j at the year i
$C_G(\tau, P)$	global cost as a function of calculation period and set of parameters [€]
CI	initial investment cost [€]
$E_{el,aux}$	electrical energy expense of auxiliary systems [kWh]
$E_{el,HP}$	electrical energy expense of heat pump [kWh]
$E_{el,tot}$	total electrical energy expense [kWh]
P	set of optimization parameters
Q_{DHW}	useful energy for domestic hot water [kWh]
Q_h	useful energy for space heating [kWh]
Q_v	useful energy for ventilation air heating [kWh]
$R_d(i)$	discount rate for year i [%]
R_R	real interest rate [%]
$V_{f,\tau}$	final value of component j at the end of calculation period [€]
w_i	weight of objective i in the multi-objective optimization function
τ	calculation period [years]

Abbreviations

AHU	air handling unit
DHW	domestic hot water
EU	European Union
GC	global cost
GHP	geothermal heat pump
HP	heat pump
INI	initial design configuration
MOB	multi-objective optimization
PSO	particle swarm optimization
SAGHP	solar assisted ground-source heat pump
SPF	seasonal performance factor
TRNSYS	transient system simulation program

various system layouts, uses and operation parameters of the storages (Schellenberg et al. 2018; Buonomano and Guarino 2020; Koşan and Aktaş 2021), which can be optimized according to different objectives (Shah et al. 2020). The TRNSYS® software has been recognized as very useful for the layout organization and simulation accuracy of the different system components (ground heat exchanger, heat pump, thermal storages, controllers, building loads, ...), as demonstrated by several studies (Desideri et al. 2011; Buonomano et al. 2015; Calise et al. 2016; Marini et al. 2019). Further, the coupling between transient simulation and artificial intelligence-based methods, such as metaheuristics optimization algorithms, has emerged for its ability to drive multiple simulation runs towards the search of optimal design configurations while analysing their performance in details in a complex set of constraints (Schellenberg et al. 2020).

However, even though recognized design guidelines exist and many different advanced models for detailed performance assessment of the different system components have been reported (Hein et al. 2016; Luo et al. 2019; Zhang et al. 2022), the operation and the long-term performance of SAGHP systems are very sensitive to the local conditions (climate, soil conditions, hydraulic parameters, energy storage ratio, etc.) (Dalla Santa et al. 2020) and should be considered for the specific set of constraints characterizing each case (D'Agostino et al. 2020). That is why populating the literature with detailed case-by-case analysis for their application in multiple different contexts is required to overcome the current barriers to the wide adoption of the technology in different climate scenarios (Ferrara et al. 2015), supported by a standardized methodological framework (Ferrara et al. 2019) for modelling and optimizing the different components and the complex set of constraints of such systems.

1.1 Aim of the work

Starting from the initial design of a system providing thermal energy for heating and DHW in the context of an Alpine ski park, this work aims at investigating the potential design optimization of a SAGHP system in a mountain site from both technical and economic points of view. To do so, the following innovation objectives will be met:

- Setup of a dedicated transient simulation-based optimization framework and definition of constraints occurring within the different variables related to thermal storages;
- Definition of key-performance indicators that can be used to set up the system multi-objective optimization to determine technical and financial feasibility;
- Dynamic exploration and multi-objective optimization of different design alternatives that are able to optimize the mutual relationship between the solar field, the geothermal field and the thermal storages;
- Quantification of potential reduction/increase of energy and cost performance within the defined design space;
- Sensitivity analysis to identify the stability of the resulting optimal design with the current uncertain financial parameters.

2 Material and methods

2.1 The case study

The case study is a SAGHP system for a newly built restaurant in a mountain site. It is located at 2500 m above the sea level in the high Alps region in rigid winter climate conditions (the annual degree days are 4524 °Cd, the mean outdoor air temperature is −3.8 °C and the winter design temperature is −20 °C). The energy demand of the building (it is expected to operate from 1st November to 30th April) was estimated through a dynamic simulation model based on real historical weather data collected in the location and typical daily occupancy schedules of similar buildings at the site. The total seasonal thermal energy demand resulting from simulation of the building model is 119027 kWh (257 kWh_{th}/m^2), of which 38.5% are needed for space heating, 50.2% for fresh air heating and 11.3% for domestic hot water production.

The system is designed to meet the building energy needs by providing water at three different thermal levels, based on user requests: (1) high temperature technical water (60 °C) to be used for air heaters and air handling units (AHU); (2) low temperature technical water for space heating radiant panels and AHU pre-heating (40 °C); (3) domestic hot water (52 °C).

As shown in Figure 1 the source-side loop is composed of a geothermal field and a hot thermal storage where a grey DHW recovery system and a solar thermal collector field are integrated with the purpose of increasing the temperature of the heat transfer fluid (water-ethylene glycol, 40%) at the evaporator side to increase the heat pump efficiency. In the initial design configuration (INI), the geothermal field is composed on 6 vertical boreholes of 200 m connected in parallel, the solar field is composed of 4 thermal collectors (2 m^2 each), the volume of the integration thermal storage is 500 l and the volume of the grey water storage is 4150 l.

The demand-side loop is composed of three water thermal storages, one for each required thermal level at the demand side. In the initial design configuration (INI), 2000 l, 1000 l and 500 l are the volumes of the high-temperature thermal storage, the low-temperature thermal storage the DHW storage, respectively. More details on the system initial design configuration can be found in Fabrizio et al. (2015).

2.2 Modelling and optimization setup

2.2.1 *Settings of simulation model*

The system dynamic simulation model was created in TRNSYS as reported in Figure 2.

To ensure model accuracy, the different model components were selected based on recognized model accuracy validation studies. The largely validated Type 1b was used for modelling flat plate solar thermal collectors (Banister et al. 2014). Type 668 was used to model the water/water heat pump through interpolation of user-defined data, based on performance curves provided by manufacturers (Dott et al. 2013). Type 557 was used to model the geothermal field (Hellstrom 1989; Ruiz-Calvo et al. 2017; Li et al. 2023) with the boreholes of diameter 40 mm and water flow rate of 0.483 l/s. The soil thermal conductivity and the soil thermal capacity were set to 1.9 W/(m·K) and 2.0 MJ/(m^3·K), respectively, and the vertical thermal gradient

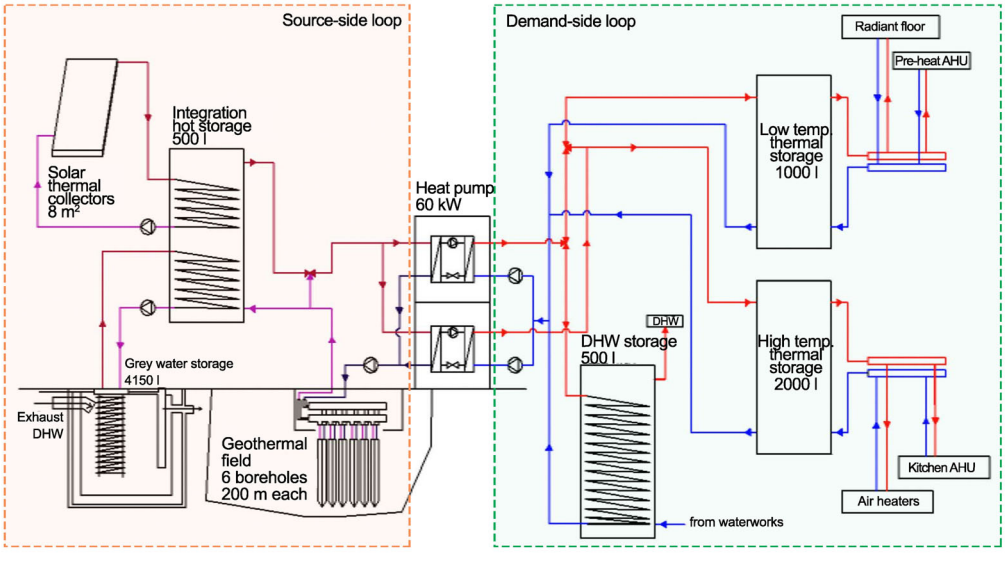

Fig. 1 System scheme in the initial design configuration

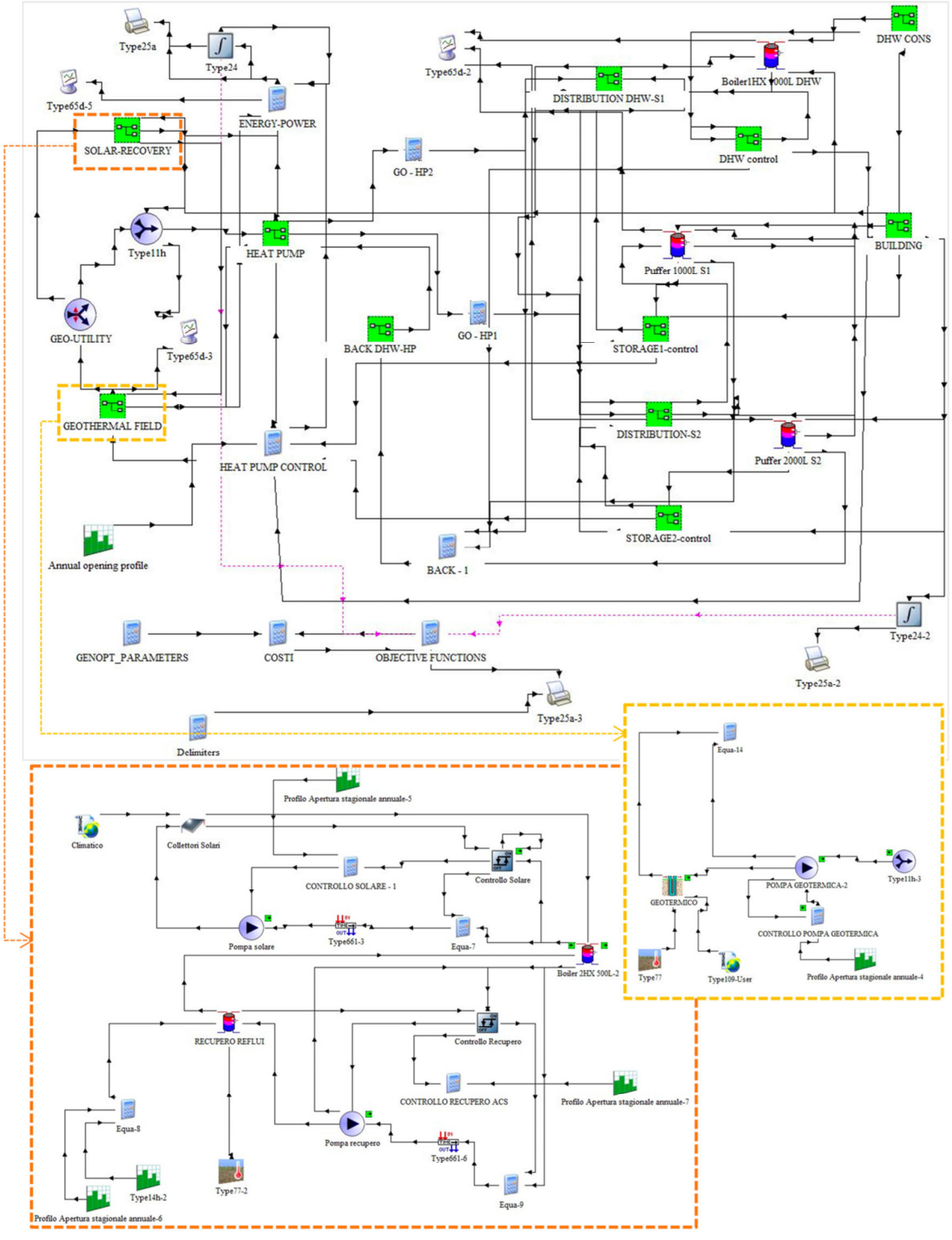

Fig. 2 System modelling network in the TRNSYS Simulation Studio interface

to 0.03 K/m. Type 60, which was demonstrated able to effectively simulate real solar water storage tanks (Johannes et al. 2005), was used to model the five stratified thermal storages included in the system. More details about the modelling and validation of other system components and control logics can be found in Urone (2015).

Once ensured the appropriate Types for the different system components were selected, the connections between different types were made based on actual system design and according to modeling approaches used in previous literature reporting the TRNSYS simulation and validation of similar solar assisted ground-source heat pump systems (Wang et al. 2012; Nam et al. 2015; Yu et al. 2016; Li et al. 2018; Sakellariou et al. 2019; Hou et al. 2020).

Based on the described TRNSYS code, the model template for the optimization was created for their use in the Genopt® software. Such template contains information on code locations where the optimization program should input the set of optimization variables, so that a seasonal TRNSYS simulation with a different system design configuration can be run at each iteration. A tailored "control center" equation type was created to properly link the user-defined set of independent optimization variables to the set of dependent variables that need to be modified and inputted to the relevant model types at each iteration (e.g. using the size of the storage volume as independent user-defined variables means modifying the entire set of geometrical parameters of the storage Type 60 – original equations and constraints were defined for the purpose, according to Table 1 and Table 2).

The optimization process was set to be driven by the binary version of particle swarm optimization (PSO) algorithm, for which the set of algorithm parameters (particles number = 5; cognitive acceleration c_1 = 3; social acceleration c_1 = 1; max swarm velocity = 4) were demonstrated to be optimal for building system optimization problems (fast convergence with high neighborhood exploration – refer to Ferrara et al. (2017) for details). The maximum number of iteration was set to 2000 for each optimization process.

2.2.2 *Optimization variables and design space*

The set of variables defining the design space for this multi-energy system optimization problem is reported in Table 1.

The range and the step for their variation is defined according to feasibility criteria (market availability, available space on the site for installation), as follows. In fact, the maximum value of the variable NColl, indicating the number of solar collectors, is set to the maximum area of the building roof that can be covered by solar collectors (considering a 2 m^2 area for each panel, the variation of NColl can increase the solar collector area up to 80 m^2). Similarly, the maximum number of geothermal boreholes is related to the available space of the geothermal site. The characteristics of thermal storages (volume and serpentine exchange surfaces) were set according to market availability. It has to be remarked that the volume of the integration hot storage is dependent on two optimization variables, one is the ratio between storage volume and solar collector area (variable STVint) and the other is the number of solar collectors (NColl), from which the solar collector area can be derived considering a 2 m^2 area for each collector. Depending on the values of the two independent variables, the volume of the integration hot storage may range between 500 l (set as minimum volume constraint) and 6000 l. The resulting 8-dimensional design space (each variable is a dimension of the design space) is composed of 5.4×10^7 points, each representing a possible design solution for the multi-energy system.

2.3 Cost functions

Cost functions representing the investment and maintenance costs for the variable system components with reference to the defined set of optimization variables (Table 1), are reported in Table 2.

An example of the process for determining cost functions is reported in Figure 2, where the total investment cost function for the integration thermal storage was derived by interpolation of real cost values for different storage sizes reported in the price lists (official price list of Valle d'Aosta Region, 2018). The so-called size-dependent costs are related to the size of the storage tank, fixed costs refer to the set of valves and pipes that are necessary for hydronic system connections, while installation costs are set to 25% of the sum of fixed and size-dependent costs, as suggested by the price lists. The linear cost function is derived as the best fit to the analysed costs (R^2 = 0.97).

Table 1 Design optimization variables

Name	Variable Description	Unit	INI	Min	Max	Step size	# steps
NColl	Number of solar thermal collectors	[–]	4	2	30	2	15
NBor	Number of geothermal boreholes	[–]	6	2	10	2	5
DBor	Depth of boreholes	[m]	200	50	350	25	12
STVint	Volume of the integration storage (solar and geothermal) per solar collectors' area	[l/m^2]	60	40	100	10	6
STVgw	Volume of the grey water storage	[l]	4000	2000	8000	1000	6
Ssol	Surface of the solar heat exchanger serpentine in the integration storage	[m^2]	2.0	2.0	4.0	0.5	5
Sgw,int	Surface of the grey water heat exchanger serpentine in the integration storage	[m^2]	3.0	3.0	7.0	0.5	8
Sgw	Surface of the heat exchanger serpentine in the grey water storage	[m^2]	7.0	3.0	9.0	1	5

Table 2 Investment cost, maintenance cost and lifespan of the system components as a function of optimization variables

Component	Involved variables	Investment cost function [€]	Maintenance [€/year]	Life span
Solar collectors	NColl	ICcoll = NColl × 2 × 563.9	MCcoll = 0.5% × ICcoll	20
Geothermal boreholes	NBor, DBor	ICbor = NBor × DBor × 76.4	MCbor = 0.5% × ICbor	30
Integration thermal storage	STVint, NColl	ICST,int = 1236.7 × (max((STVint × NColl × 2), 500)) + 834.6	MCST,int = 1% × ICST,int	20
Grey water thermal storage	STVgw	ICST,w = 971.7 × (STVw) + 528.0	MCST,w = 1% × ICST,w	20

Regarding thermal storages, the cost analysis based on price lists, and confirmed by manufacturers, has highlighted that only the volume and the number of serpentines (two heat exchanger serpentines are included in the integration hot storage, one is included in the grey water storage) have direct impact on the investment cost, if the heat exchange surface area of serpentines is maintained within feasible ranges. Therefore, cost functions of thermal storages only depend on optimization variables related to storage volume (variables STVint, STVw) and, in case of integration hot storage, on the number of solar collectors, because of the interdependency between STVint and NColl. That is why the cost function in Figure 3 is defined considering the storage volume as the x independent variable. In the model, as reported in Table 2, such volume is determined as the product of STVint and the total area of solar collectors, obtained by multiplying NColl by the single collector area (2 m^2), with a minimum value of 500 l set as a constraint.

2.4 Objective functions

According to Standard EN 15459 for economic evaluation of energy systems in buildings (CEN 2017), the global cost has been considered as the primary objective of this study, as follows:

$$C_G(\tau,P) = \mathrm{CI} + \sum_j \left[\sum_{i=1}^{\tau} \left(C_{a,i}(j) \times R_d(i) \right) - V_{f,\tau}(j) \right] \text{[€]} \quad (1)$$

where C_G (τ, P) represents the global cost relatively to the starting year τ_0, considering a number τ of years as the calculation period and the defined set of design variables P, CI is the initial investment cost, $C_{a,i}(j)$ is the annual cost for component j at the year i (including running costs and periodic or replacement costs), $R_d(i)$ is the discount rate for year i, $V_{f,\tau}$ (j) is the final value of component j at the end of the calculation period (relatively to the starting year τ_0).

The calculation period of 30 years and the financial parameters were initially set according to EU guidelines for performing cost-optimal analysis (European Commission 2012) following Directive 2010/31/EU (Market interest rate 4.5%, inflation rate 2%, real interest rate 2.5%, rate of evolution of energy price 2%). Lower real interest rates (R_R = 1.5% and R_R = 0.5%) deriving from different combinations of market and inflation rates reflecting the EU macroeconomic context of the last decade were also considered to perform a sensitivity analysis to financial parameters.

With respect to the other macroeconomic parameters, energy prices may be subject to much higher variability in the very short and medium term, due to the unstable availability of energy sources and their strict relation with social and political contexts. Therefore, following official statistics about energy prices in the European Union in view of the current international political context, which is likely to have a very important impact on the current and future energy prices (https://ec.europa.eu/eurostat/web/energy/database), a dedicated sensitivity analysis was

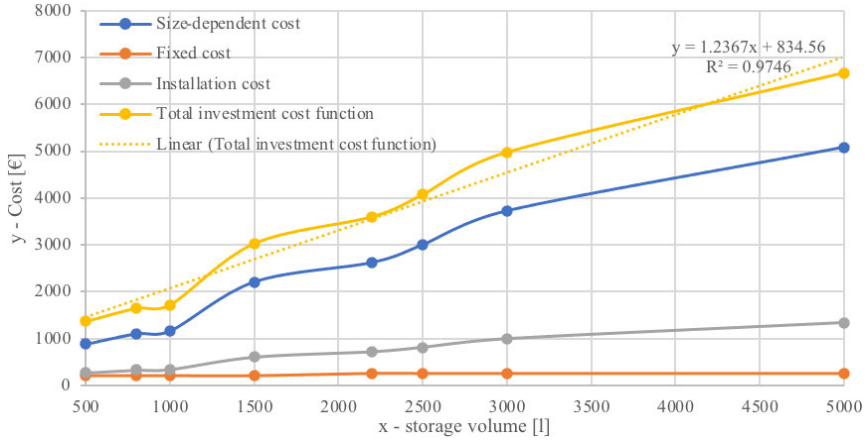

Fig. 3 Example of cost function for a thermal storage tank

conducted on the rate of development of energy prices. In particular, the rate of development of electricity price R_e was considered and the sensitivity of results to the increase of such rate up to R_e = 10% was investigated (in the very last years many countries have been experiencing such average increase of energy prices, including Italy).

It is important to note that this global cost objective function is directly influenced by the energy performance itself, as lower energy use is related to lower running costs, included in the global cost computation. However, energy costs are associated to purchased energy from the grid but may not be representative of the efficiency of the system. Therefore, the seasonal performance factor of the system was also evaluated to better understand the energy performance in terms of system efficiency. It was defined, as used for multipurpose systems, the ratio of the total useful energy output to the total energy expense of a system (Zottl and Nordman 2012; Biglia et al. 2021) as follows:

$$\mathrm{SPF}_{\mathrm{SAGHP}} = \frac{Q_h + Q_v + Q_{\mathrm{DHW}}}{E_{\mathrm{el,HP}} + E_{\mathrm{el,aux}}} \quad [—] \tag{2}$$

where Q_h, Q_v and Q_{DHW} are the useful energy outputs for space heating, ventilation and DHW, while $E_{el,HP}$ and $E_{el,aux}$ are the electrical energy inputs for the heat pump operation and the auxiliary systems (circulation pumps).

Given these two objectives, a multi-objective optimization function can be written as follows:

$$\mathrm{MOF}_{\mathrm{SAGHP}} = w_1 \frac{C_G - C_{G,\min}}{C_{G,\max} - C_{G,\min}} + w_2 \frac{\mathrm{SPF} - \mathrm{SPF}_{\max}}{\mathrm{SPF}_{\min} - \mathrm{SPF}_{\max}} \quad [—] \tag{3}$$

where $\mathrm{MOF}_{\mathrm{SAGHP}} \in [0, 1]$. Weights w_1 and w_2 can be assigned to the two objectives according to user-defined priority, provided that $w_1 + w_2 = 1$. In this study $w_1 = w_2 = 0.5$.

3 Results

3.1 System modelling results

The adopted model setup resulted to be able to correctly simulate the system operation according to the initial design specifications. Figure 4 reports several model outputs for four example days of operation (January 14th to 17th). In details, describing Figure 4 from bottom to top, it is possible to see the modelled dynamic operation of the different parts of the system by means of the dynamic trend of several simulated variables.

Regarding the external environment, it is shown that the external dry bulb air temperature (T_ext [°C]) is quite rigid and often below 0 °C, demonstrating the need for heat pump sources with higher temperatures than air, such as the geothermal source, of which the average temperature is shown to be around 6 °C [T_ave_geo [°C]). It is also shown that the solar radiation (Solar_rad [W/m²]) is available during opening hours when higher thermal loads occur (Q_tot [kW]), showing the opportunity to use the solar source for further increasing the source temperature of the heat pump. The dynamics of thermal loads for the different uses (Q_AHU – heating load for air handling units operation [kW_{th}], Q_radiant floor – heating load for radiant floor operation [kW_{th}]; Q_DHW – heating load for domestic hot water [kW_{th}]) show the accuracy of the model according to the expected operating conditions (smaller heating loads at night are required for the radiant floor operating in antifreeze conditions).

Thermal loads are also reflected in the dynamics of temperatures in the three load-side storages where the variable T_storage_highT represents the average fluid temperature in the high-temperature storage dedicated to the air handling units loop, T_storage_lowT is the average fluid temperature in the low-temperature storage dedicated to the radiant floor loop and T_storage_DHW is the average temperature in the storage dedicated to domestic hot water.

Such oscillating dynamics of storages show the correct simulation of the degree-minute-based control logic for the operation of the heat pump. Its intermittent operation is driven by the entity and speed of temperature decrease in the load-side storages and is shown through the dynamics of the electric power demand of the double-stage heat pump (P_ele_HP – [kW_{el}]) and of thermal capacities absorbed at the evaporator and delivered at the condensator (Q_source_HP and Q_load_HP, respectively [kW_{th}] – peaks represent the call for second stage of operation).

Regarding the operating conditions of the storages at the source side, the graph at the top of Figure 4 shows in details the different temperature levels at the different points of the loop and the contribution of the solar and the greywater sources to increase the temperature in the integration hot storage (see system scheme in Figure 1). In details:

- T_in_geo – temperature of the fluid entering the geothermal field [°C];
- T_in_STint – temperature of the fluid coming from the geothermal field and entering the integration hot storage, waiting for gaining additional heat from the solar and grey water sources [°C];
- T_out_STint – temperature of the fluid at the outlet of the integration hot storage, ready for transferring heat to the heat pump evaporator [°C];
- T_ave_STgw – average water temperature in the grey water storage [°C];
- Q_fromHXsol – heat transferred to the integration hot storage from the solar loop [kW];

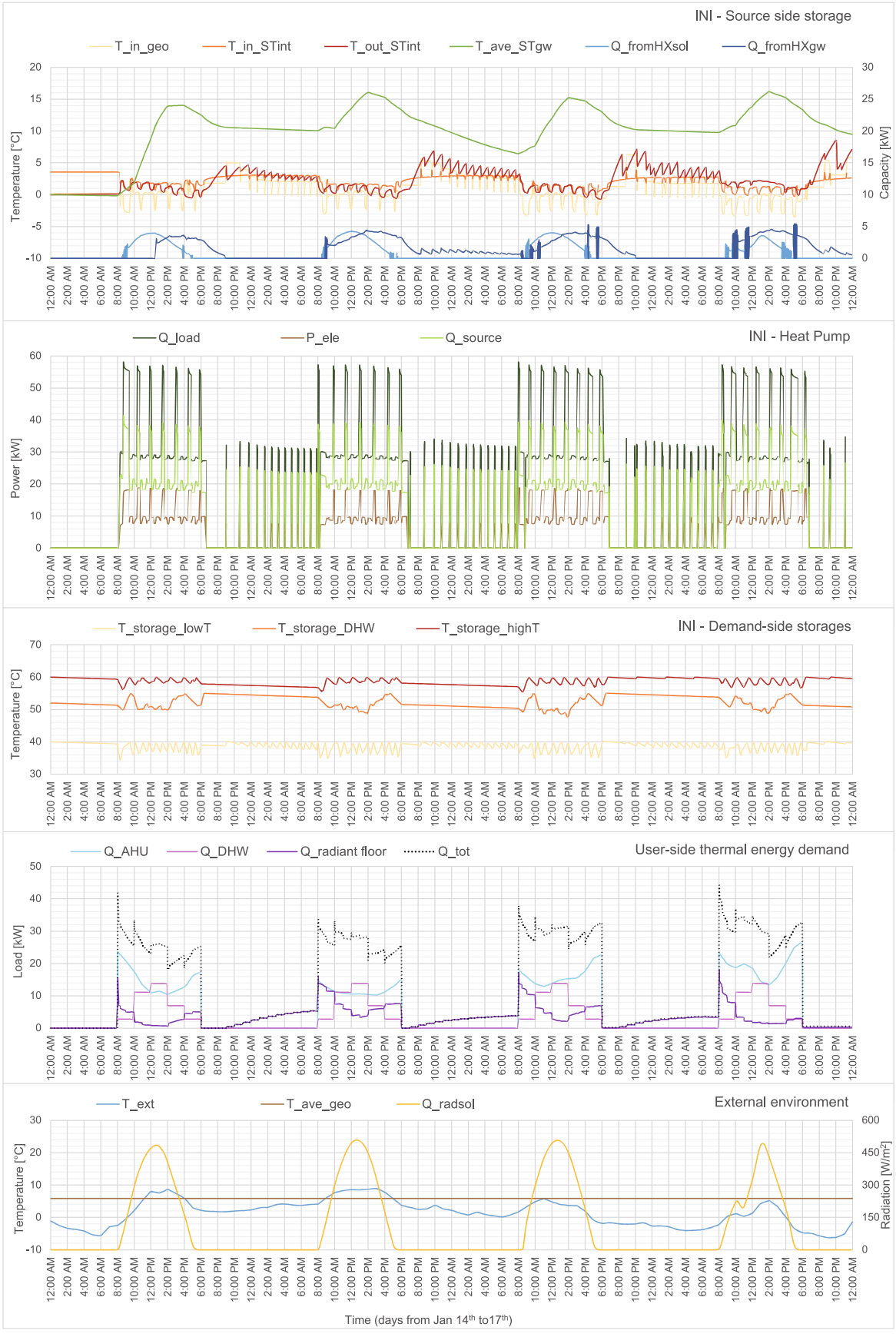

Fig. 4 Four sample days of dynamic operation of the modelled system in its initial configuration

- Q_fromHXgw – heat transferred to the integration hot storage from the grey water loop [kW].

These results have been compared to previous studies where similar systems were modelled in TRNSYS, as described in Section 2. Despite the differences due to the different boundary conditions and component sizing referring to each particular case study, the obtained simulation outputs are consistent with expectations based on system design features and with simulation outputs resulting in other studies reported in the literature. In particular, it is shown that the oscillating temperature levels of the fluids entering and exiting the borehole heat exchangers and entering in the heat pump follows the on-off operation of the heat pump and related call for storage discharge, similarly to a previous study reporting outputs of a similar TRNSYS model (Li et al. 2018). The same study reports a similar behavior of temperatures in water storages. Coherently with the outputs reported in a previous study regarding the operation of a SAGHP in a cold climate (Rad et al. 2013), the average temperature increase is around 3 °C in the initial configuration, where a recent study demonstrating that the output of such modelling approach may lead to a small underestimation of temperature of the fluid exiting the ground heat exchanger (0.05 °C). However, as mentioned, the reults reported in Figure 4 refer to sample days for the system operation in its initial design configuration (blue point in Figure 5) and should be interpreted as typical trends for the all involved and interrelated output variables, rather than absolute results. These are shown as an example of the correct operation and good accuracy of the model, but these are subject to variation for the optimized system configurations, which will be shown in the next result subsection.

3.2 Optimization results

The entire set of evaluated design alternatives, reported in Figure 5, were obtained within the four single-objective optimization runs to minimize and maximize the two objectives (global cost and seasonal performance factor, Eqs. (1) and (2)) and the final multi-objective optimization run (Eq. (3)). Each point of Figure 5 represents a different design alternative, reported in a graph where the global cost is reported on the vertical axis and the SPF is reported on the horizontal axis. Further than the point minimizing the multi-objective function (MOBopt, orange dot), other notable points were highlighted, such as the minimum and the maximum achievable SPF (green and red dots for SPFmin and SPFmax, respectively) and the minimum and the maximum achievable global cost (violet and light blue dots for GCmin and GCmax, respectively). The initial design configuration (INI) is represented in blue. The different sets of design variable values for the highlighted notable points are reported in Table 3, together with the related values of global cost, SPF and non-renewable energy expense ($E_{el,tot}$, that is the denominator of Eq. (2)).

Results show that, within the design space delimited by the defined set of parameters, the global cost may vary between 179023 € and 523423 € (−13.7% and +152% with respect to the initial design solution), while the SPF may vary between 3.66 and 3.88 (−0.5% and + 5% with respect to the initial design solution). The minimum global cost is achieved with SPF that is slightly higher than the minimum, while the maximum SPF is only achievable with higher increase of global cost. However, the minimization of the multi-objective optimization function shows that it is possible to identify a solution leading to nearly optimal SPF

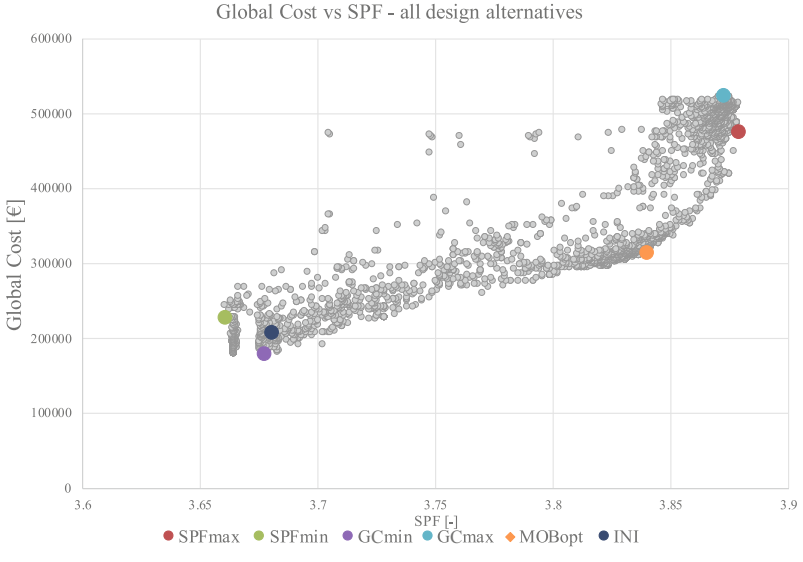

Fig. 5 Global cost vs SPF of all evaluated design alternatives and notable points

Table 3 Design configuration and related objective function values in optimal and notable points

Name	Unit	INI	GCmin	GCmax	SPFmin	SPFmax	MOBopt
NColl	[—]	4	2	30	2	8	18
NBor	[—]	6	1	10	3	10	4
DBor	[m]	200	50	350	200	350	350
STVint	[l/m^2]	50	100	100	50	40	70
STVgw	[l]	4000	2000	8000	3000	5000	2000
Ssol	[m^2]	2.5	2.5	3.5	2	3.5	3.5
Sgw,int	[m^2]	3.5	6.0	7.0	5.5	3.5	6.0
Sgw	[m^2]	7.0	9.0	6.0	9.0	9.0	9.0
Global cost	[€]	207457	179023	523423	227722	474736	313983
SPF	[—]	3.68	3.68	3.85	3.66	3.88	3.84
$E_{el,tot}$	[kWh]	32337	32369	30733	32516	30683	30995

but significant reduction of global cost (−34%).

The analysis of the resulting optimal values of design variables in the different notable points shows that the global cost is highly influenced by the investment cost, which greatly increases when the number and the deep of the borehole increase, without causing a significant increase in energy performance and a consequent significant reduction of operational costs that is able to impact the overall global cost calculation. From the energy performance point of view, it is shown that the initial design configuration INI has almost the same low performance level of the resulting cost-optimal solution, but even with a high number of solar field and significant increase of the geothermal field the achievable increase of SPF is around 6%.

However, such performance increase can be appraised by studying the dynamics of the different system variables. Figure 6 shows the dynamics of the variables related to the source-side loop in the SPFopt and the MOBopt point for the same sample days already reported in Figure 4. The temperatures of the fluid at the different loop points is reported (T_in_geo, T_in_STint, T_out_STint, T_ave_STgw), showing the ability of the system setup to effectively increase the thermal levels of the fluid thanks to the different heat sources and therefore increase the overall system performance.

If compared to the trends in Figure 4, it is shown that, in both optimized system configurations SPFopt and MOBopt, the temperature of the fluid exiting the integration storage (T_out_STint) is increased of about 3.5°C on average with respect to the INI configuration (Figure 3). However, the temperature dynamics is different due to greater exploitation of the geothermal field in the SPFopt configuration, while the MOBopt relies more on the exploitation of a greater solar field, as also shown by the variable Q_fromHXsol in Figure 6. This is also coherent with the resulting optimal value of optimization variables reported in Table 3. Both SPFopt and MOBopt are also able to make the contribution of the heat recovery from waste greywater increase with respect to the INI configuration.

4 Discussion

4.1 Analysis of the optimum neighborhood

Beyond the absolute results in terms of energy and cost performance (the dependent variables), the relative relationship between one and the other design alternative should be considered, with the resulting optimal values of the selected optimization variables to be implemented in the real design (the independent variables). In this context, the analysis of the points located in the neighborhood of notable and/or optimal points may give important information about the robustness of the resulting optimal design solutions against uncertainty of modelling inputs and outputs, as also emerging from other applications of the EDeSSOpt methodology (Ferrara et al. 2018, 2020).

Therefore, the set of optimization variables related to different design alternatives falling in the the neighborhoods of the GCmin and the MOBopt points were studied.

The neighborhoods where defined considering a 10% maximum distance from optimum values of the relevant objective functions. The neighborhood of GCmin resulted to be composed of 216 points, with GC lower than 196925 € and SPF ranging between 3.66 and 3.70, while 440 points were included in the neighborhood of MOBopt, where the 10% deviation from minimum MOB value led to identify a part of the Pareto front where SPF ranges between 3.81 and 3.87 for global cost values ranging between 298283 € and 361080 € (Figure 7).

The graphs in Figure 8 and Figure 9 show the distribution of the frequency of values of optimization variables occurring in the points composing the neighborhoods. The fact that, for

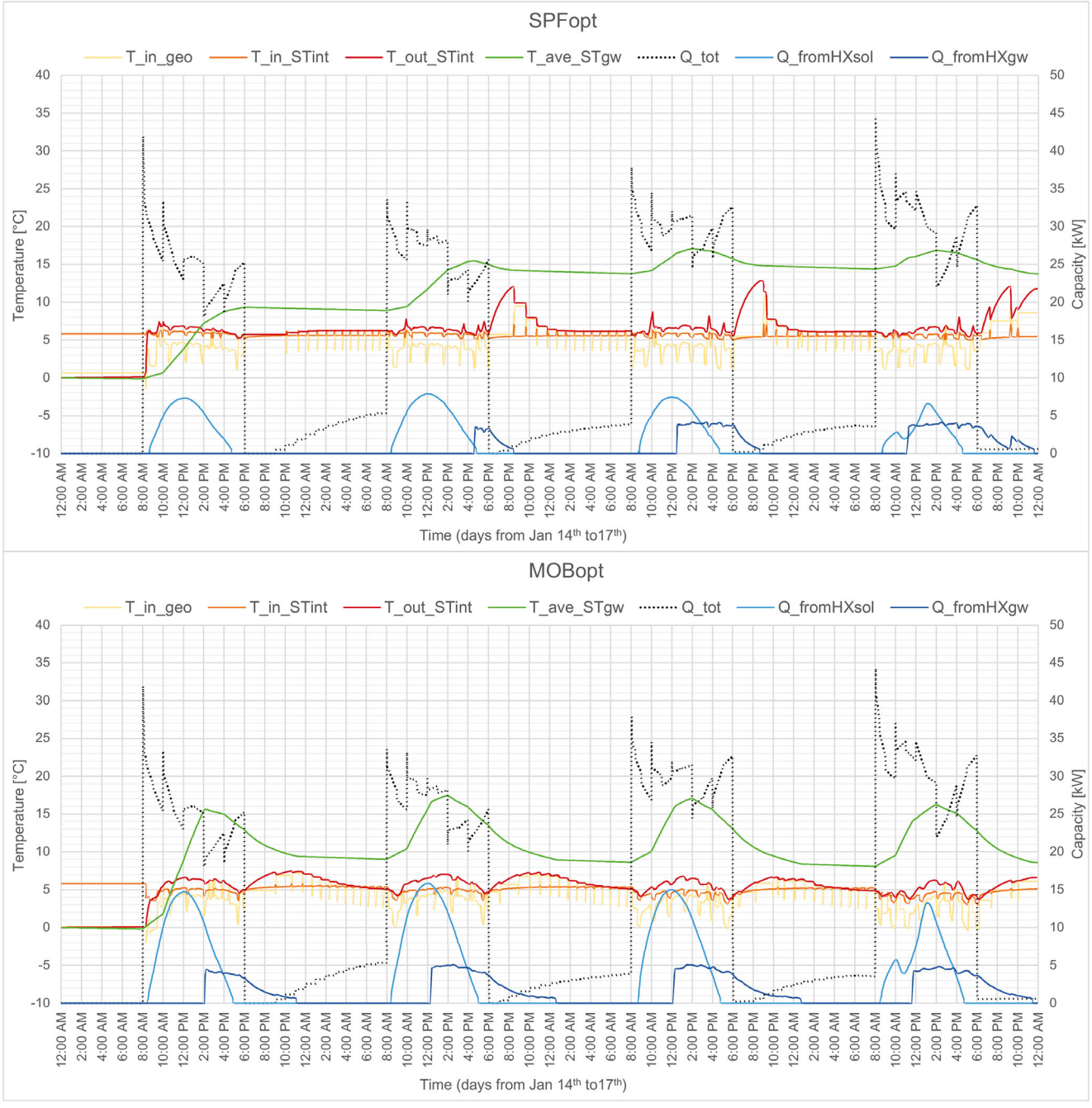

Fig. 6 Dynamics of source-side variables in four sample days for the SPFopt and MOBopt optimized system configurations (T_in_geo – temperature of the fluid entering the geothermal field [°C]; T_in_STint – temperature of the entering the integration hot storage[°C]; T_out_STint – temperature of the fluid at the outlet of the integration hot storage [°C]; T_ave_STgw – average water temperature in the grey water storage [°C]; Q_fromHXsol – heat transferred to the integration hot storage from the solar loop [kW]; Q_fromHXgw – heat transferred to the integration hot storage from the grey water loop [kW], Q_tot –total heating loads)

an optimization variable, most points in the neighborhood have the same values as the optimal point means that the variable is significant – if that variable is not optimized in a design alternative, it is likely to fall outside the optimum neighborhood.

Regarding the neighborhood of GCmin (details in Figure 8), it is shown that the main design variables have high level of robustness as most design alternatives in the neighborhood have a low number of solar collectors and a low number of boreholes (depth appears as not significant). Regarding storages, it is shown that the volume of the integration hot storage (driven by variable STVint) should stay low, as a consequence of the low number of solar collectors. On the other hand, it is shown that the volume

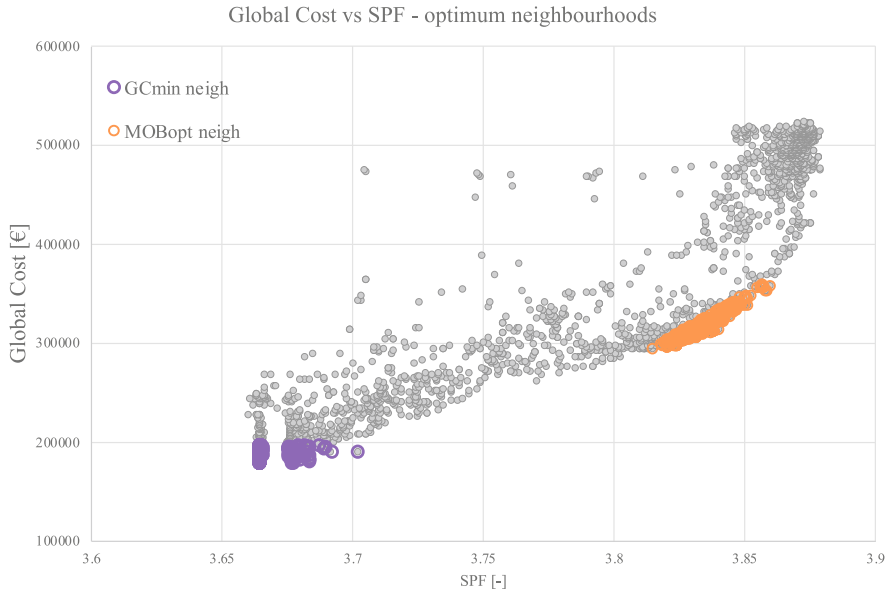

Fig. 7 Neighborhoods of optimal points GCmin and MOBopt

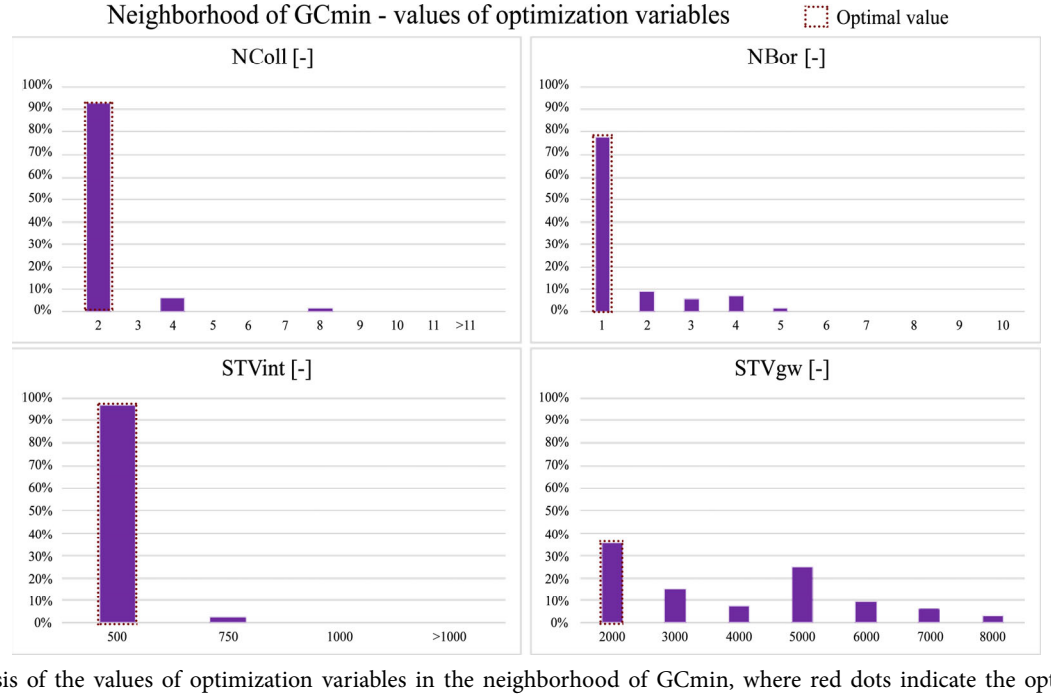

Fig. 8 Analysis of the values of optimization variables in the neighborhood of GCmin, where red dots indicate the optimal variable values in the GCmin point

of the greywater storage (driven by variable STVgw) is not a driver for the optimality. The proper sizing of the integration hot storage should have priority over the size of the greywater storage in order to ensure the cost-optimality of the real design.

Different results are shown in Figure 9, where the analysis of values of optimization variables in the neighborhood of MOBopt is reported. In fact, only the NBor variable presents a high level of robustness. It is shown that the other variables may assume almost all values in the defined variability range while leading to the neighborhood of the minimum value of the multi-objective function. In other words, it is shown that many different design configurations may lead to similar results and therefore the final decision may be made following other criteria.

4.2 Sensitivity analysis

Figure 10 reports the results obtained from the analysis of sensitivity to financial parameters. As shown, design

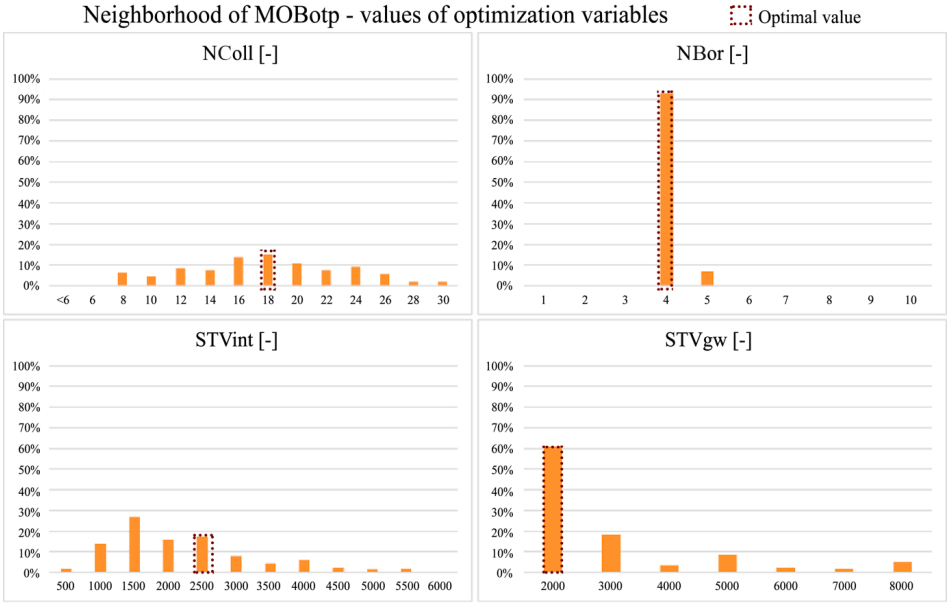

Fig. 9 Analysis of the values of optimization variables in the neighborhood of MOBopt, where red dots indicate the optimal variable values in the MOBopt point

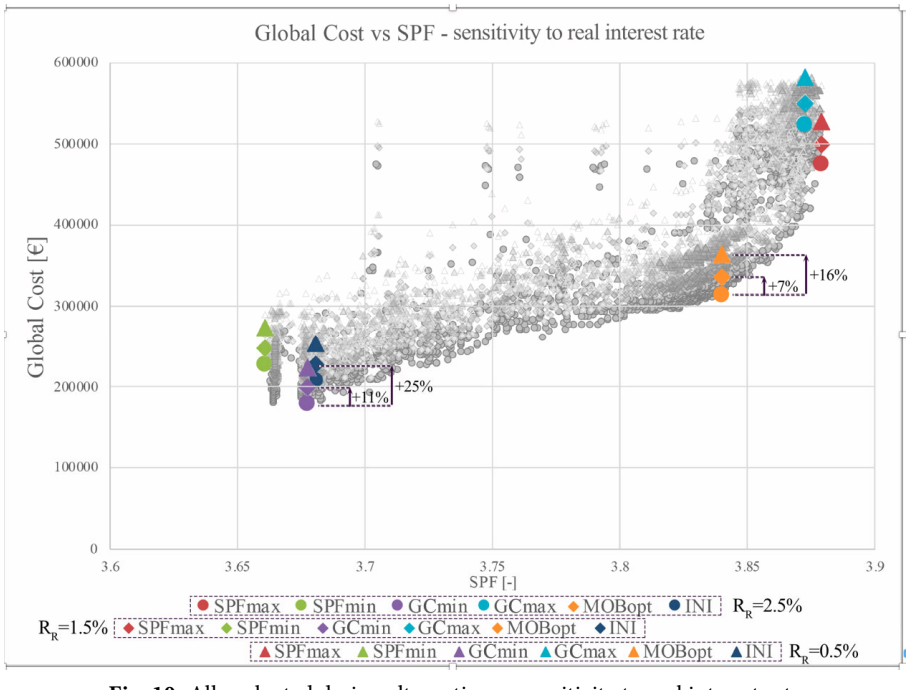

Fig. 10 All evaluated design alternatives – sensitivity to real interest rate

configurations of optimal and notable points do not change due to variation of real interest rate (the same optimizations that were initially run with R_R of 2.5% were then run with R_R of 1.5% and 0.5%). These results demonstrate a high stability of the obtained optimal design solutions with respect to variation of financial parameters. However, lower real interest rates may lead to increase the global cost values, for which the present study quantifies up to 16% (for MOBopt solution) or 25% (for GCmin solution).

Figure 11 reports the results obtained from the analysis of sensitivity to the rate of development of energy prices R_e when the other financial parameters are set to their initial value (R_R set to 2.5% following European guidelines). Also in this case, the relative position of one point with respect to the others is not subject to substantial variations, meaning that design configurations of optimal and notable points and their related neighborhoods are stable with respect to the rate of development of energy prices (the same

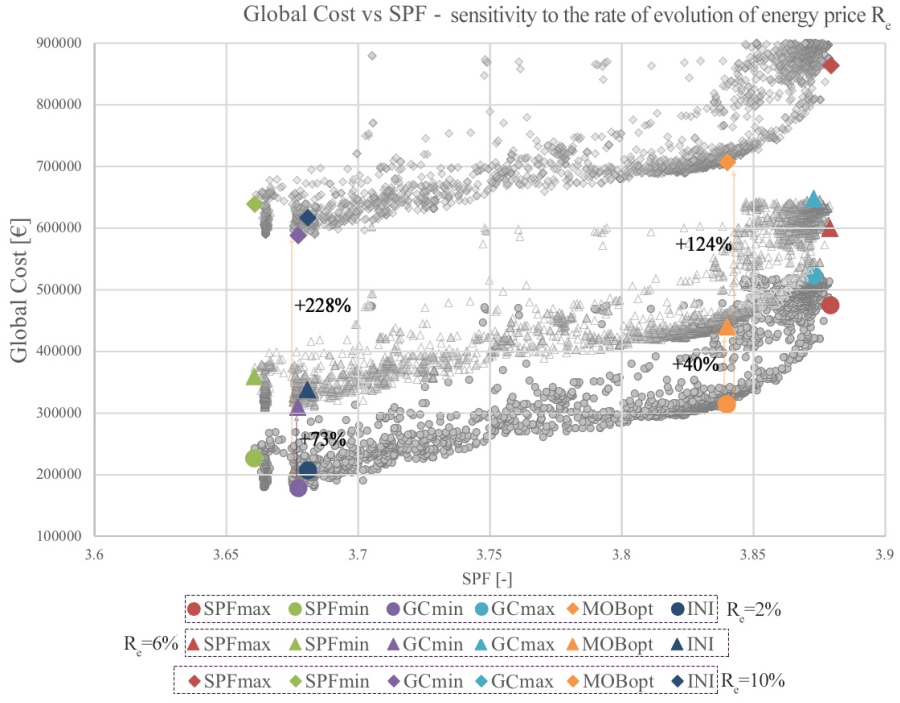

Fig. 11 All evaluated design alternatives – sensitivity to the rate of development of energy prices

optimizations that were initially run with R_e of 2% were then run with R_e of 6% and 10%).

As in previous case, these results confirm a high level of robustness of the obtained optimal design solutions with respect to variation of financial parameters.

This means that it is possible to design and implement a system configuration that is optimized in the current economic context and it is likely to stay optimal even in case of quite high variation of financial parameters. However, the higher development shows very high increase of global cost values, for which the present study quantifies up to 228% (for GCmin solution) or 124% (for MOBopt solution). Therefore, in case of high development of energy price rates a much lower relative variation of global cost values with respect to initial design solution can be appraised. In fact, in case of R_e = 10%, the global cost may vary between 588534 € and 912244 € in absolute terms, that is −4% and +48% in relative terms with respect to the initial design solution, with the MOBopt solution leading to increase the global cost by only 14% with respect to the initial design configuration (it was +51% with the basic assumption of the rate of development of energy prices).

In an economic context when the rate of development of energy price is expected to be subject to very high increase, this approach may lead to change the final design choice in favour of a more energy efficient design configuration, despite it is clear that, within the defined set of constraints, investment costs will account for the higher weight on the global cost even if the weight of energy cost increases.

5 Conclusions

The design of a real SAGHP system for a building in the Alps region was modelled in detail and optimized from both energy performance and cost points of view. The simulation model resulted to be effective to support the understanding of the dynamics of the different parts of the multi-energy systems and appraising the impact of design variation on the behavior of each component and of the overall system, as well as the mutual relationship between the solar field, the geothermal field and the thermal storages. In particular, a new dedicated simulation-based optimization framework was created with a tailored set of optimization variables, providing accurate definition of modeling constraints occurring within the different variables related to thermal storages. With respect to the initial design solution, the study demonstrated a potential reduction of global cost of 13.7% for the same energy performance, or a potential increase of seasonal performance factor of about 6% at the expense of very high increase of global cost.

This means that such a system configuration can reach valuable performance (similar to that achieved from similar systems in other contexts), if properly optimized and integrated with available renewable sources, also in extreme context of environmental conditions, therefore demonstrating the wide applicability of the heat pump technology towards worldwide decarbonization. Moreover, the performed sensitivity analysis showed high level of robustness of the resulting optimal solution with respect to financial parameters

and even with the current high development of energy prices, demonstrating the reliability of the performed technical studies even in context of financial and economic uncertainty, while highlighting the need for incentive policies that are able to increase the weight of energy costs in the calculated global cost and therefore increase financial feasibility of this type of system.

In general, beyond the numerical results that can drive design of such systems in similar contexts, the paper highlights the potential of dynamic simulation and optimization to support the complex design of multi-source multi-energy systems and shows the possibility to identify trade-off design solutions driven by KPIs that are representative of technical and financial objectives. The presented approach and original setup of simulation-based optimization framework for the thermal storage design parameters can be replicated for modelling and optimizing the other similar multi-energy multi-source systems with different set of external constraints.

Further work should be performed to include control strategies in the set of optimization variables, especially regarding control of thermal storages, in order to explore further possibilities for improving energy performance without causing investment cost increases.

Funding note: Open access funding provided by Politecnico di Torino within the CRUI-CARE Agreement. Funding to Maria Ferrara's activity was provided by Italian MUR within the PON "Ricerca e Innovazione" 2014–2020, Asse IV "Istruzione e ricerca per il recupero" – Azione IV.4 – "Dottorati e contratti di ricerca su tematiche dell'innovazione" e Azione IV.6 – "Contratti di ricerca su tematiche Green".

Declaration of competing interest

The authors have no competing interests to declare that are relevant to the content of this article.

Author contribution statement

All authors contributed to the study conception and design, in the framework of IEA ESTCP Annex/Task 37 activities. Material preparation, data collection and analysis were performed by Maria Ferrara. The first draft of the manuscript was written by Maria Ferrara and all authors commented on previous versions of the manuscript. All authors read and approved the final manuscript.

References

Alberti L, Antelmi M, Angelotti A, et al. (2018). Geothermal heat pumps for sustainable farm climatization and field irrigation. *Agricultural Water Management*, 195: 187–200.

Banister CJ, Wagar WR, Collins MR (2014). Validation of a single tank, multi-mode solar-assisted heat pump TRNSYS model. *Energy Procedia*, 48: 499–504.

Biglia A, Ferrara M, Fabrizio E (2021). On the real performance of groundwater heat pumps: experimental evidence from a residential district. *Applied Thermal Engineering*, 192: 116887.

Buonomano A, Calise F, Palombo A, et al. (2015). Energy and economic analysis of geothermal-solar trigeneration systems: A case study for a hotel building in Ischia. *Applied Energy*, 138: 224–241.

Buonomano A, Guarino F (2020). The impact of thermophysical properties and hysteresis effects on the energy performance simulation of PCM wallboards: experimental studies, modelling, and validation. *Renewable and Sustainable Energy Reviews*, 126: 109807.

Calise F, Dentice d'Accadia M, Figaj RD, et al. (2016). Thermoeconomic optimization of a solar-assisted heat pump based on transient simulations and computer Design of Experiments. *Energy Conversion and Management*, 125: 166–184.

CEN (2017). EN 15459—Energy performance of buildings—Economic evaluation procedure for energy systems in buildings.

D'Agostino D, Minichiello F, Valentino A (2020). Contribution of low enthalpy geothermal energy in the retrofit of a single-family house: a comparison between two technologies. *Journal of Advanced Thermal Science Research*, 7: 30–39.

Dalla Santa G, Galgaro A, Sassi R, et al. (2020). An updated ground thermal properties database for GSHP applications. *Geothermics*, 85: 101758.

Desideri U, Sorbi N, Arcioni L, et al. (2011). Feasibility study and numerical simulation of a ground source heat pump plant, applied to a residential building. *Applied Thermal Engineering*, 31: 3500–3511.

Dott R, Afjei T, Genkinger A, et al (2013). Models of Sub-Components and Validation for the IEA SHC Task 44 /HPP Annex 88 - Part C: Heat Pump models (subtask C report).

European Commission (2012). Guidelines accompanying Commission Delegated Regulation (EU) No 244/2012 of 16 January 2012 supplementing Directive 2010/31/EU of the European Parliament and of the Council on the energy performance of buildings by establishing a comparative methodology framework for calculating cost-optimal levels of minimum energy performance requirements for buildings and building elements.

Fabrizio E, Ferrara M, Urone G, et al. (2015). Performance assessment of a solar assisted ground source heat pump in a mountain site. *Energy Procedia*, 78: 2286–2291.

Ferrara M, Fabrizio E, Virgone J, et al. (2015). Appraising the effect of the primary systems on the cost optimal design of nZEB: A case study in two different climates. *Energy Procedia*, 78: 2028–2033.

Ferrara M, Dabbene F, Fabrizio E (2017). Optimization Algorithms Supporting the Cost-Optimal Analysis: The Behavior of PSO. In: Proceedings of the 15th IBPSA International Building Simulation Conference, San Francisco, USA.

Ferrara M, Sirombo E, Fabrizio E (2018). Energy-optimized versus cost-optimized design of high-performing dwellings: the case of multifamily buildings. *Science and Technology for the Built Environment*, 24: 513–528.

Ferrara M, Prunotto F, Rolfo A, et al. (2019). Energy demand and supply simultaneous optimization to design a nearly zero-energy house. *Applied Sciences*, 9: 2261.

Ferrara M, Lisciandrello C, Messina A, et al. (2020). Optimizing the transition between design and operation of ZEBs: lessons learnt from the Solar Decathlon China 2018 SCUTxPoliTo prototype. *Energy and Buildings*, 213: 109824.

Girard A, Gago EJ, Muneer T, et al. (2015). Higher ground source heat pump COP in a residential building through the use of solar thermal collectors. *Renewable Energy*, 80: 26–39.

Hein P, Kolditz O, Görke UJ, et al. (2016). A numerical study on the sustainability and efficiency of borehole heat exchanger coupled ground source heat pump systems. *Applied Thermal Engineering*, 100: 421–433.

Hellstrom G (1989). Duct Ground Heat Storage Model, Manual for Computer Code.

Hou G, Taherian H, Li L (2020). A predictive TRNSYS model for long-term operation of a hybrid ground source heat pump system with innovative horizontal buried pipe type. *Renewable Energy*, 151: 1046–1054.

International Energy Agency (2020). Energy Technology Perspectives.

Johannes K, Fraisse G, Achard G, et al. (2005). Comparison of solar water tank storage modelling solutions. *Solar Energy*, 79: 216–218.

Koşan M, Aktaş M (2021). Experimental investigation of a novel thermal energy storage unit in the heat pump system. *Journal of Cleaner Production*, 311: 127607.

Li H, Xu W, Yu Z, et al. (2018). Discussion of a combined solar thermal and ground source heat pump system operation strategy for office heating. *Energy and Buildings*, 162: 42–53.

Li Y, Bi Y, Lin Y, et al. (2023). Analysis of the soil heat balance of a solar-ground source absorption heat pump with the soil-based energy storage in the transition season. *Energy*, 264: 126394.

Liu X, Spitler JD, Qu M, et al. (2021). Recent developments in the design of vertical borehole ground heat exchangers for cost reduction and thermal energy storage. *Journal of Energy Resources Technology*, 143: 100803.

Luo Y, Guo H, Meggers F, et al. (2019). Deep coaxial borehole heat exchanger: Analytical modeling and thermal analysis. *Energy*, 185: 1298–1313.

Marini D, Buswell RA, Hopfe CJ (2019). Sizing domestic air-source heat pump systems with thermal storage under varying electrical load shifting strategies. *Applied Energy*, 255: 113811.

Maturo A, Buonomano A, Athienitis A (2022). Design for energy flexibility in smart buildings through solar based and thermal storage systems: Modelling, simulation and control for the system optimization. *Energy*, 260: 125024.

Nam Y, Gao X, Yoon S, Lee K (2015). Study on the performance of a ground source heat pump system assisted by solar thermal storage. *Energies*, 8: 13378–13394.

Nouri G, Noorollahi Y, Yousefi H (2019). Solar assisted ground source heat pump systems—A review. *Applied Thermal Engineering*, 163: 114351.

Osterman E, Stritih U (2021). Review on compression heat pump systems with thermal energy storage for heating and cooling of buildings. *Journal of Energy Storage*, 39: 102569.

Ozgener O, Hepbasli A (2007). A review on the energy and exergy analysis of solar assisted heat pump systems. *Renewable and Sustainable Energy Reviews*, 11: 482–496.

Rad FM, Fung AS, Leong WH (2013). Feasibility of combined solar thermal and ground source heat pump systems in cold climate, Canada. *Energy and Buildings*, 61: 224–232.

Rivoire M, Casasso A, Piga B, et al. (2018). Assessment of energetic, economic and environmental performance of ground-coupled heat pumps. *Energies*, 11: 1941.

Ruiz-Calvo F, Montagud C, Cazorla-Marín A, et al. (2017). Development and experimental validation of a TRNSYS dynamic tool for design and energy optimization of ground source heat pump systems. *Energies*, 10: 1510.

Sakellariou EI, Wright AJ, Axaopoulos P, et al. (2019). PVT based solar assisted ground source heat pump system: modelling approach and sensitivity analyses. *Solar Energy*, 193: 37–50.

Schellenberg C, Lohan J, Dimache L (2018). Operational optimisation of a heat pump system with sensible thermal energy storage using genetic algorithm. *Thermal Science*, 22: 2189–2202.

Schellenberg C, Lohan J, Dimache L (2020). Comparison of metaheuristic optimisation methods for grid-edge technology that leverages heat pumps and thermal energy storage. *Renewable and Sustainable Energy Reviews*, 131: 109966.

Shah SK, Lu A, Rismanchi B (2020). Multi-objective optimisation of a seasonal solar thermal energy storage system for space heating in cold climate. *Applied Energy*, 268: 115047.

Urone G (2015). Modeling of a solar assisted geothermal heat pump for a high-altitude accommodation facility. Politecnico di Torino. (in Italian)

Wang E, Fung AS, Qi C, et al. (2012). Performance prediction of a hybrid solar ground-source heat pump system. *Energy and Buildings*, 47: 600–611.

Wołoszyn J, Gołaś A (2017). Coefficient of performance stabilisation in ground source heat pump systems. *Journal of Sustainable Development of Energy, Water and Environment Systems*, 5: 645–656.

Yu M, Nam Y, Yu Y, et al. (2016). Study on the system design of a solar assisted ground heat pump system using dynamic simulation. *Energies*, 9: 291.

Zhang C, Nielsen E, Fan J, Furbo S (2022). Thermal behavior of a combi-storage in a solar-ground source heat pump system for a single-family house. *Energy and Buildings*, 259: 111902.

Zottl A, Nordman R (2012). D4.2. /D 2.4. Concept for evaluation of SPF. Version 2.2. Tech. rep.of the SEPEMO-BUILD Project.